Auger-electron spectrum of atomic cesium in the 15–75-eV energy range

Helena Aksela and Seppo Aksela
Department of Physics, University of Oulu, SF-90570 Oulu 57, Finland
(Received 8 February 1983)

Auger-electron spectrum of Cs in the 15–75-eV energy region following 20 keV electron impact is presented. The most intensive structures in the spectra are analyzed by comparing their energies with the calculated energies of the Auger transitions applying a multiconfiguration Dirac-Fock method. Also the free-atom binding energies $E_B(N_5)=82.79.\pm0.10$ eV and $E_b(N_4)=85.07\pm0.10$ eV are obtained with the aid of optical double-hole final-state energy levels.

I. INTRODUCTION

The ejected-electron spectra of barium vapor at the low-energy regions, which contain several autoionization and Auger lines, have been reported recently.[1–3] In this work we have studied the next lower element, cesium, in the vapor phase. After ionization in the 4*s*, 4*p*, or 4*d* levels by bombardment with 2-keV electrons, the Auger decay leads to a rich fine structure in the ejected-electron spectrum in the measured 15–17-eV energy range.

The collapse of the 5*d* and 4*f* wave functions in the 4*d* excited atomic Cs and the *s*-*d* mixing effects were studied theoretically by Connerade.[4–6] The 4*d* excited Cs was observed to be very sensitive to the influence of the effects due to both the 6*s*-5*d* correlation and wave-function collapse. The analysis of the ejected-electron spectrum of Cs allows us to study the magnitude of the collapse and the correlation effects in the singly ionized initial and the doubly ionized final states of the 4*s*, 4*p*, and 4*d* Auger transitions.

II. EXPERIMENTAL

The spectra have been measured by means of a cylindrical mirror spectrometer and with the use of electron-beam excitation.[7] The spectrometer is equipped with a resistance-heated high-temperature oven system. Owing to the higher vapor pressure of Cs, only slight heating of the oven was needed to produce the pressure of about 10^{-1} Pa inside the oven, where the primary beam crossed the vapor target. A standard pulse counting method was used and the pulses were collected into the memory of a microprocessor, which was also used to control the spectrometer voltages.[8] The energy resolution of the spectrometer was about 0.1%, and the Auger lines of Kr (Ref. 9) were used for the energy calibration, with the correction of 0.20 eV proposed by Ohtani *et al.*[10] and Hansen and Persson.[11]

The experimental spectrum of Cs excited with 2-keV electrons in the 15–70-eV energy range is shown in Figs. 1 and 2. The energy region 70–75 eV had no clear peak structure, and it was left therefore outside the range of the figures. In addition to the subtraction of a constant background of 26 000 counts per channel, a linear background ranging from 3000 counts on the left-hand side to zero on the right was also subtracted from the spectrum shown in Fig. 1. When the electrostatic energy analyzers are used without preretardation, the energy window selected by the slits is proportional to the kinetic energy. The spectrum must therefore be multiplied by a factor proportional to the inverse of the kinetic energy before the intensities of the different lines can be determined. The dispersion-corrected spectrum is shown in Fig. 2. The lines were then fitted by the least-squares method, using Voigt functions as the standard line shapes. The fit is shown by the solid line in Fig. 2, and the energies, intensities, and linewidths obtained from the fit are given in Table I. The

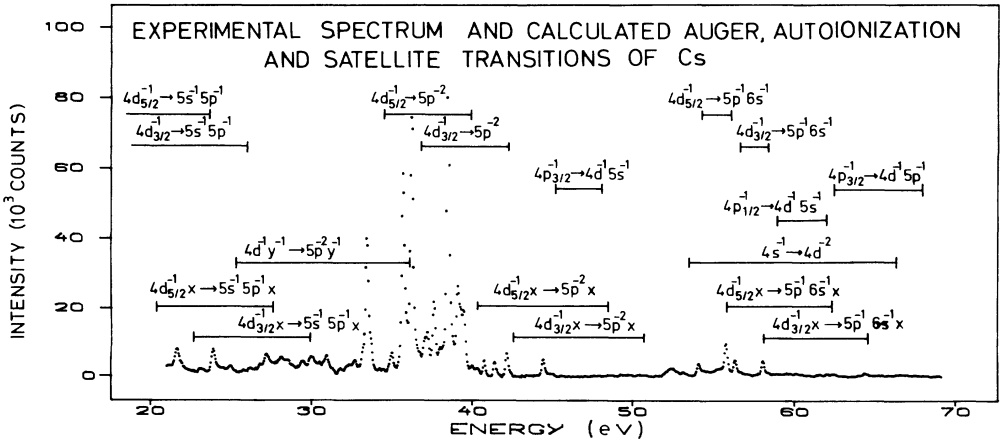

FIG. 1. Experimental Auger-electron spectrum of atomic cesium after background subtraction. Energies of Auger, autoionization, and satellite transitions are from Dirac-Fock calculations.

TABLE I. Experimental energies (in eV), intensities (in %), and linewidths (in eV) of the Auger-electron lines of the cesium atom.

Line number in Fig. 2	Energy	Intensity	Linewidth	Transition
1	16.61	0.74	0.2	$4d^{-1}_{3/2,5/2} \rightarrow 5s^{-1}5p^{-1}$ Auger lines
2	17.10	0.56	0.2	$4d^{-1}y^{-1} \rightarrow 5p^{-2}y^{-1}$ satellite lines
3	17.38	0.81	0.2	$4d^{-1}x \rightarrow 5s^{-1}5p^{-1}x$ autoionizaton
4	17.73	1.73	0.4	
5	18.08	0.67	0.4	
6	18.53	1.01	0.4	
7	18.80	0.80	0.4	
8	19.03	0.84	0.4	
9	19.41	0.45	0.4	
10	20.71	1.12	0.4	
11	21.09	1.23	0.4	
12	21.69	4.39	0.4	
13	22.37	0.66	0.4	
14	23.22	0.46	0.2	
15	23.98	1.84	0.2	
16	24.42	0.69	0.4	
17	24.99	0.84	0.4	
18	25.80	0.08	0.2	
19	26.25	0.51	0.4	
20	26.83	0.66	0.4	
21	27.27	2.26	0.4	
22	27.80	0.96	0.4	
23	28.19	1.56	0.4	
24	28.54	1.21	0.4	
25	28.91	0.47	0.4	
26	29.44	1.31	0.4	
27	30.01	1.84	0.4	
28	30.45	0.74	0.4	
29	30.94	1.84	0.4	
30	31.82	0.31	0.2	$4d^{-1}_{3/2,5/2} \rightarrow 5p^{-2}$ Auger lines
31	32.38	1.10	0.4	energy-loss peaks
32	32.73	0.54	0.2	
33	33.37	1.55	0.2	
34	33.48	5.83	0.2	
35	34.27	0.18	0.2	
36	34.50	0.15	0.2	
37	34.98	0.94	0.2	
38	35.73	8.76	0.2	
39	36.26	11.44	0.2	

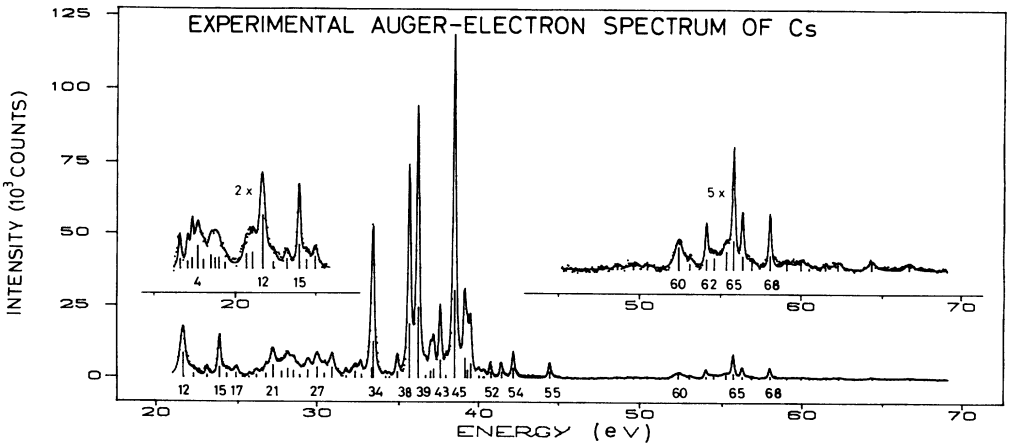

FIG. 2. Auger-electron spectrum of atomic cesium after background subtraction and dispersion correction. Solid curve and vertical lines represent a least-squares fit of Voigt functions to the experimental points.

TABLE I. (*Continued.*)

Line number in Fig. 2	Energy	Intensity	Linewidth	Transition
40	36.74	0.40	0.2	
41	37.05	1.12	0.2	
42	37.23	1.45	0.2	
43	37.65	2.89	0.2	
44	37.99	0.42	0.2	
45	38.52	14.22	0.2	
46	39.16	3.19	0.2	
47	39.32	1.24	0.2	
48	39.51	2.29	0.2	
49	40.03	0.34	0.2	
50	40.30	0.16	0.2	
51	40.35	0.16	0.2	
52	40.75	0.63	0.2	
53	41.42	0.67	0.2	$4d^{-1}x \rightarrow 5p^{-2}x$ autoionization
54	42.17	1.12	0.2	
55	44.42	0.68	0.2	
56	47.70	0.03	0.6	$4p_{3/2}^{-1} \rightarrow 4d^{-1}5s^{-1}$ Auger lines
57	48.62	0.11	0.6	$4d^{-1}y^{-1} \rightarrow 5p^{-1}x^{-1}y^{-1}$ satellite lines
58	49.61	0.15	0.6	
59	50.47	0.11	0.6	
60	52.38	0.72	0.6	
61	53.06	0.20	0.6	$4d_{3/2,5/2}^{-1} \rightarrow 5p^{-1}x^{-1}$ Auger lines
62	54.09	0.34	0.2	energy-loss peaks
63	54.56	0.38	0.6	
64	55.31	0.59	0.6	
65	55.76	0.93	0.2	
66	56.32	0.45	0.2	
67	56.89	0.25	0.6	
68	58.04	0.46	0.2	
69	59.09	0.24	0.6	$4p_{1/2}^{-1} \rightarrow 4d^{-1}5s^{-1}$ Auger lines
70	59.98	0.23	0.6	$5s^{-1} \rightarrow 4d^{-2}$ Auger lines
71	60.50	0.07	0.6	
72	61.54	0.11	0.6	
73	62.32	0.18	0.6	
74	64.41	0.23	0.6	$4p_{3/2}^{-1} \rightarrow 4d^{-1}5p^{-1}$ Auger lines
75	66.76	0.18	0.6	$4s^{-1} \rightarrow 4d^{-2}$ Auger lines

linewidths also contain the contribution from instrumental broadening. The binding energies of the $4d$ levels were obtained by adding the optically known final-state energy[12] of the $5s^2 5p^5\,{}^2P^o_{3/2}$ level of Cs III to the determined kinetic energies of the corresponding Auger lines (lines 65 and 68 in Fig. 2). Thus the values $E_B(N_4)=85.07\pm0.10$ eV and $E_B(N_5)=82.79\pm0.10$ eV were obtained in excellent agreement with the photoabsorption measurements of Petersen *et al.*[13]

III. CALCULATIONS

Multiconfiguration Dirac-Fock calculations have been performed in order to obtain the energies of the singly and doubly ionized and excited states of Cs atom. The energies have been computed using the Dirac-Fock code of Grant *et al.*[14] The program is able to solve the atomic multiconfiguration Dirac-Fock equations and supply the energy levels. The transverse Breit, self-energy, and vacuum polarization corrections are also included in the calculated values of the energy levels.[14]

A. Initial states of Auger decay

In order to obtain the energies of the initial states of the Auger transitions, the $4s^{-1}$, $4p^{-1}$, and $4d^{-1}$ configura-

TABLE II. Mean radii of the 6s, 5d, and 4f wave functions (in a.u.) in neutral, singly, and doubly ionized states of Cs.

Wave function	Neutral Cs	Mean radii $4p^{-1}$	$4d^{-1}$	$5p^{-2}$
6s	6.1	4.6	4.6	4.1
$5d_{3/2}$	7.7	3.3	3.4	2.9
$5d_{5/2}$	17.1	3.4	3.5	3.1
$4f_{5/2}$		7.9	8.1	2.2
$4f_{7/2}$		7.9	8.2	2.3

tions were considered. The 4d Auger transitions have more intensity than the 4s and 4p Auger transitions, due to the larger number of electrons. The $4d^{-1}$ initial states were therefore examined first in detail.

Single-configuration calculations for the $4d^{-1}6s$, $4d^{-1}5d$, and $4d^{-1}4f$ configurations showed a small energy difference of 1.0 eV between the first two configurations, whereas the $4d^{-1}4f$ configuration was found to deviate by 5.7 eV towards higher binding energies from the $4d^{-1}6s$ configuration. The near degeneracy of the $4d^{-1}6s$ and $4d^{-1}5d$ configurations was then treated by admixing these configurations to the atomic state $4d^{-1}(6s+5d)$ with the use of the multiconfiguration approach. Owing to the different parities, the $4d^{-1}(6s+5d)$ and $4d^{-1}4f$ states do not mix with each other. The first one, being energetically more advantageous, is thus the proper description for the initial state of the 4d Auger decay. The energy splitting in the initial state, due to electrostatic interaction with the open outer shell, was found to be 0.04 eV for the $4d^{-1}6s$ configuration and 0.9 eV for the $4d^{-1}5d$ configuration.

In the consideration of the $4p^{-1}$ initial states the configurations $4p^{-1}6s$, $4p^{-1}5d$, and $4p^{-1}4f$ were observed at distances of 0.7 and 5.0 eV from each other. The decrease of the energy difference between the above-mentioned initial-state configurations in passing from the $4d^{-1}$ hole state to the $4p^{-1}$ hole state clearly demonstrates the sensitivity of the collapse of the 5d and 4f wave functions to the change in the states of the other electrons. The mean radii of the 5d and 4f wave functions also decrease respectively, as can be seen from Table II. However, in a manner analogous to the $4d^{-1}$ initial state, the $4p^{-1}$ initial state is also well described by the $4p^{-1}(6s+5d)$ atomic state. Owing to the small intensity of the 4s Auger transitions, only one single-configuration ($4s^{-1}6s$) calculation was carried out for this initial state

B. Final states of Auger decay

In the measured energy region the final states of the 4d Auger transitions are $5s^{-1}5p^{-1}$, $5p^{-2}$, $5s^{-1}x^{-1}$, and $5p^{-1}x^{-1}$, where $x=6s$, 5d, or 4f. In a manner analogous to the initial state, the single-configuration and multiconfiguration computations were also carried out for these final states. The increase in the ionization degree clearly manifests itself as an increase in the collapse of the wave functions (Table II), although the ionization now takes place on the outermost shells.

The final state $5p^{-1}x^{-1}$ ($x=6s$, 5d, or 4f) consists of two lines according to the quantum numbers $J=\frac{1}{2}$ and $\frac{3}{2}$. The fine structure arising from the $5p^{-2}$ and $5s^{-1}x^{-1}$ final states overlap energetically. The splitting of the "parent lines" of the $5p^{-2}$ and $5s^{-1}5p^{-1}$ configurations into the "daughters" caused by the presence of the outer 6s, 5d, or 4d electron is illustrated in Fig. 3, where the energies of the 4d Auger lines are presented in each case. The multiconfiguration results are also shown. Figure 3 clearly shows the increase in the number of lines and in the spread of the splitting in passing from the $5p^{-2}6s$ configuration to the $5p^{-2}5d$ configuration and further to the $5p^{-2}4f$ configuration. The absolute energies of the lines given in Fig. 3 are obtained as a difference between the initial- and final-state energies (Δ SCF approach).

The $4p^{-1}\rightarrow 4d^{-1}5s^{-1}$ and $4s^{-1}\rightarrow 4d^{-2}$ Auger transi-

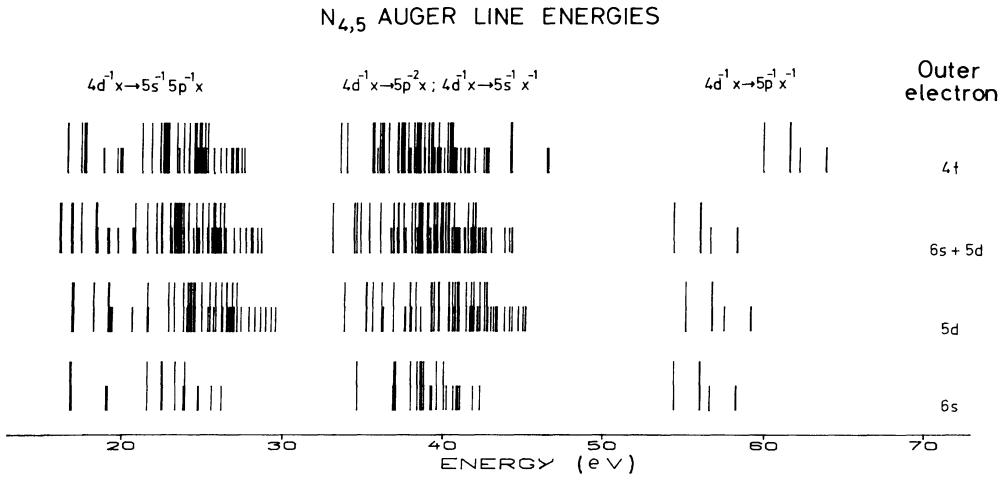

FIG. 3. Energies of the 4d Auger lines of Cs calculated with the Dirac-Fock Δ SCF method. Single-configuration results with 4f, 6s, or 5d outer electron and multiconfiguration results with $6s+5d$ mixing are presented. Higher lines refer to the N_5 transitions and lower lines to the N_4 transitions.

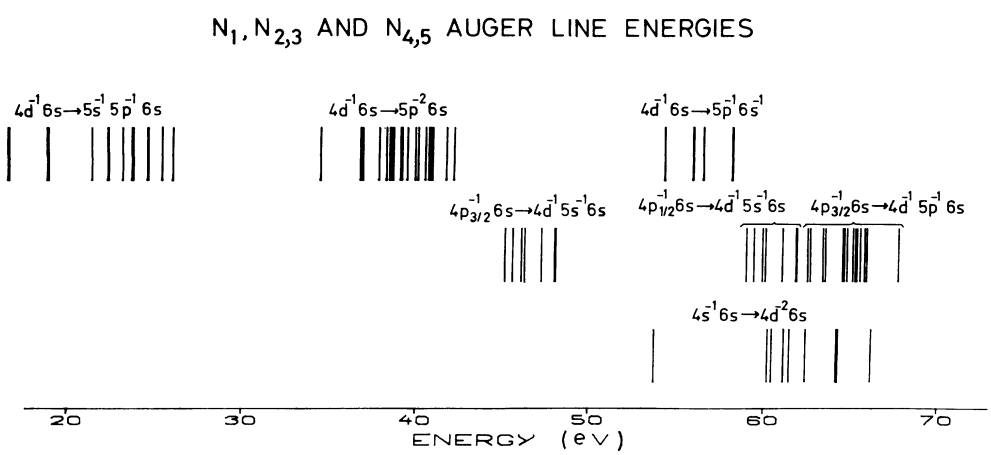

FIG. 4. Energies of the $4d$, $4p$, and $4s$ Auger lines of Cs obtained from the single-configuration (with $6s$ outer electron) Dirac-Fock Δ SCF computations.

tions were found to lie energetically in the high-energy part of the spectrum. The $4d$, $4p$, and $4s$ Auger transitions, according to the single-configuration computations with the $6s$ outer electron, are shown in Fig. 4. The energy regions are also given in Fig. 1 together with the experimental spectrum.

C. Autoionization

Instead of ionization, excitation can also take place in the cesium atom when bombarded with electrons. This leads to transitions of the autoionization type. In order to obtain the energy regions of these transitions, their initial and final states were computed: In the initial state the electron was excited to the $5d$, $6s$, or $4f$ level. In the final state two electrons were missing from the $5s$, $5p$, or x ($x=6s$, $5d$, or $4f$) levels of the excited atom. The energies of the autoionization lines obtained as a difference between the initial- and final-state energies are shown together with the calculated normal Auger line energies and the experimental spectrum in Fig. 1.

IV. DISCUSSION

A comparison between the experimental spectrum and the calculated energy positions depicted in Fig. 1 shows that the most intensive lines in the spectrum are clearly due to the $4d$ Auger transitions. The four sharp lines in the energy region 54—58 eV (lines 62, 65, 66, and 68 in Fig. 2) can easily be identified as corresponding to the $4d^{-1}_{3/2,5/2}\rightarrow 5p^{-1}x^{-1}$, $J=\frac{1}{2}$ and $\frac{3}{2}$ transitions. A comparison between the calculated and measured kinetic energies shows an energy difference of the order of 0.4 eV between theory and experiment. This difference is probably due to the fact that the interaction with the continuum in the initial state has not been included in the computations.[15] The intensity ratio of the first two lines to the last two is found to be 1.4, which corresponds reasonably well to the statistical distribution of holes in the initial state. According to the energy calculations shown in Fig. 4, the $4p^{-1}\rightarrow 4d^{-1}5s^{-1}$ transitions fall energetically within the same energy regions as the $4d^{-1}\rightarrow 5p^{-1}x^{-1}$ transitions. Furthermore, the $4s^{-1}\rightarrow 4d^{-1}4d^{-1}$ transitions lie on the high-energy side of both of these transitions. Because the final state $4d^{-1}$ of both of these transitions can further decay by the $4d$ Auger process, the lines are considerably broadened. Broader linewidths were, indeed, obtained from the fit of the experimental spectrum for all the other high-energy lines except the lines 62, 65, 66, and 68, which were interpreted as the $4d^{-1}\rightarrow 5p^{-1}x^{-1}$ Auger lines. The calculated energy positions of the $4p$ and $4s$ Auger lines

TABLE III. The $N_{4,5}O_{2,3}P_1$ Auger lines of Cs atoms. The calculated energies without parentheses are Dirac-Fock Δ SCF (energy-difference) results. The energies of the loss peaks (in parentheses) are obtained by subtracting 1.4 eV (Ref. 15) from the main peak.

Line number in Fig. 2	Energy Expt.	Calc.	Interpretation
61	53.06	(52.94)	Loss peak of line 62; satellite
62	54.09	54.34	$4d^{-1}_{5/2}\rightarrow 5p^{-1}_{1/2}6s^{-1}$, $J=\frac{1}{2}$
63	54.56	(54.61)	Loss peak of line 65
64	55.31	(55.20)	Loss peak of line 66; satellite
65	55.76	56.01	$4d^{-1}_{5/2}\rightarrow 5p^{-1}_{3/2}6s^{-1}$, $J=\frac{3}{2}$
66	56.32	56.60	$4d^{-1}_{3/2}\rightarrow 5p^{-1}_{1/2}6s^{-1}$, $J=\frac{1}{2}$
67	56.89	(56.87)	Loss peak of line 68
68	58.04	58.27	$4d^{-1}_{3/2}\rightarrow 5p^{-1}_{3/2}6s^{-1}$, $J=\frac{3}{2}$

TABLE IV. $N_{4,5}O_{2,3}O_{2,3}$ Auger lines of the CS atom. The calculated energies without parentheses are Dirac-Fock ΔSCF results. The main contributions to the final-state wave functions are given in the last column. The energies of the loss peaks (in parentheses) are obtained by subtracting 1.4 eV (Ref. 15) from the main peak.

Line number in Fig. 2	Energy Expt.	Energy Calc.	Interpretation
31	32.38	(33.16)	Loss peak from line 34 satellite line
32	32.73	(33.16)	Loss peak from line 34 satellite line
33	33.37	34.41	$4d_{5/2}^{-1}\rightarrow -0.7[5p_{1/2}^{-1}5p_{3/2}^{-1}(J=2)5d_{5/2},J=\frac{1}{2}\rangle -0.4[5p_{1/2}^{-1}5p_{3/2}^{-1}(J=2)5d_{3/2},J=\frac{1}{2}\rangle +0.4[5p_{1/2}^{-2}(J=0)6s,J=\frac{1}{2}\rangle$
34	33.48	34.56	$4d_{5/2}^{-1}\rightarrow -0.8[5p_{1/2}^{-2}(J=0)6s,J=\frac{1}{2}\rangle -0.4[5p_{3/2}^{-2}(J=0)6s,J=\frac{1}{2}\rangle -0.3[5p_{1/2}^{-1}5p_{3/2}^{-1}(J=2)5d_{3/2}^{-1},J=\frac{1}{2}\rangle$
35	34.27	(35.42)	Loss peak from line 38
36	34.50	(35.42)	Loss peak from line 38
37	34.98	(35.44)	Loss peak from line 39
38	35.73	36.82	$4d_{3/2}^{-1}\rightarrow -0.8[5p_{1/2}^{-2}(J=0)6s,J=\frac{1}{2}\rangle -0.4[5p_{3/2}^{-2}(J=0)6s,J=\frac{1}{2}\rangle -0.3[5p_{1/2}^{-1}5p_{3/2}^{-1}(J=2)5d_{3/2}^{-1},J=\frac{1}{2}\rangle$
39	36.26	36.88	$4d_{5/2}^{-1}\rightarrow -0.9[5p_{3/2}^{-2}(J=2)6s,J=\frac{3}{2}\rangle -0.3[5p_{1/2}^{-1}5p_{3/2}^{-1}(J=2)6s,J=\frac{3}{2}\rangle$ $4d_{5/2}^{-1}\rightarrow 0.9[5p_{1/2}^{-1}5p_{3/2}^{-1}(J=2)6s,J=\frac{5}{2}\rangle -0.3[5p_{3/2}^{-2}(J=2)6s,J=\frac{5}{2}\rangle -0.3[5p_{1/2}^{-1}5p_{3/2}^{-1}(J=2)5d_{5/2},J=\frac{5}{2}\rangle$
40	36.74		Energy-loss or satellite line
41	37.05	37.20	$4d_{5/2}^{-1}\rightarrow 0.7[5p_{1/2}^{-1}5p_{3/2}^{-1}(J=2)5d_{3/2},J=\frac{1}{2}\rangle -0.6[5p_{1/2}^{-1}5p_{3/2}^{-1}(J=2)5d_{5/2},J=\frac{1}{2}\rangle -0.3[5p_{1/2}^{-2}(J=0)6s,J=\frac{1}{2}\rangle$
42	37.23	(36.74)	Loss peak from line 45
43	37.65	38.02	$4d_{5/2}^{-1}\rightarrow 0.9[5p_{1/2}^{-1}5p_{3/2}^{-1}(J=1)6s,J=\frac{1}{2}\rangle -0.3[5p_{3/2}^{-2}(J=0)6s,J=\frac{1}{2}\rangle$
44	37.99	38.22	$4d_{5/2}^{-1}\rightarrow -0.9[5s^{-1}6s^{-1},J=\frac{1}{2}\rangle +0.4[5p_{3/2}^{-2}(J=0)6s,J=\frac{1}{2}\rangle$ $4d_{5/2}^{-1}\rightarrow 0.9[5p_{1/2}^{-1}5p_{3/2}^{-1}(J=1)6s,J=\frac{3}{2}\rangle -0.3[5p_{1/2}^{-1}5p_{3/2}^{-1}(J=2)5d_{5/2},J=\frac{3}{2}\rangle$ Loss peak from line 46
45	38.52	39.14	$4d_{3/2}^{-1}\rightarrow -0.9[5p_{3/2}^{-2}(J=2)6s,J=\frac{3}{2}\rangle -0.3[5p_{1/2}^{-1}5p_{3/2}^{-1}(J=2)6s,J=\frac{3}{2}\rangle$ $4d_{3/2}^{-1}\rightarrow 0.9[5p_{1/2}^{-1}5p_{3/2}^{-1}(J=2)6s,J=\frac{5}{2}\rangle -0.3[5p_{3/2}^{-2}(J=2)6s,J=\frac{5}{2}\rangle -0.3[5p_{1/2}^{-1}5p_{3/2}^{-1}(J=2)5d_{5/2},J=\frac{5}{2}\rangle$

TABLE IV. (*Continued.*)

Line number in Fig. 2	Energy Expt.	Energy Calc.	Interpretation
46	39.16	39.44	$4d_{5/2}^{-1} \rightarrow 0.8[5p_{3/2}^{-2}(J=2)6s, J=\frac{3}{2}\rangle - 0.3[5p_{1/2}^{-1}5p_{3/2}^{-1}(J=1)5d_{5/2}, J=\frac{3}{2}\rangle + 0.3[5p_{1/2}^{-1}5p_{3/2}^{-1}(J=1)5d_{3/2}, J=\frac{3}{2}\rangle$
47	39.32	39.46	$4d_{3/2}^{-1} \rightarrow 0.7[5p_{1/2}^{-1}5p_{3/2}^{-1}(J=2)5d_{3/2}, J=\frac{1}{2}\rangle - 0.6[5p_{1/2}^{-1}5p_{3/2}^{-1}(J=2)5d_{5/2}, J=\frac{1}{2}\rangle - 0.3[5p_{1/2}^{-2}(J=0)6s, J=\frac{1}{2}\rangle$
48	39.51	40.28	$4d_{5/2}^{-1} \rightarrow -0.8[5p_{3/2}^{-2}(J=2)6s, J=\frac{5}{2}\rangle + 0.3[5p_{3/2}^{-2}(J=0)5d_{5/2}, J=\frac{5}{2}\rangle$
49	40.03	40.28	$4d_{3/2}^{-1} \rightarrow 0.9[5p_{1/2}^{-1}5p_{3/2}^{-1}(J=1)6s, J=\frac{1}{2}\rangle - 0.3[5p_{3/2}^{-2}(J=0)6s, J=\frac{1}{2}\rangle$
50	40.30	40.48	$4d_{3/2}^{-1} \rightarrow 0.9[5p_{1/2}^{-1}5p_{3/2}^{-1}(J=1)6s, J=\frac{3}{2}\rangle - 0.3[5p_{1/2}^{-1}5p_{3/2}^{-1}(J=2)5d_{5/2}, J=\frac{3}{2}\rangle$
51	40.35	40.83	$4d_{3/2}^{-1} \rightarrow -0.9[5s^{-1}6s^{-1}, J=\frac{1}{2}\rangle + 0.4[5p_{3/2}^{-2}(J=0)6s, J=\frac{1}{2}\rangle$
52	40.75	40.95	$4d_{3/2}^{-1} \rightarrow -0.8[5p_{3/2}^{-2}(J=0)6s, J=\frac{1}{2}\rangle + 0.4[5p_{1/2}^{-2}(J=0)6s, J=\frac{1}{2}\rangle$
53	41.42	41.70	$4d_{3/2}^{-1} \rightarrow 0.8[5p_{3/2}^{-2}(J=2)6s, J=\frac{3}{2}\rangle - 0.3[5p_{1/2}^{-1}5p_{3/2}^{-1}(J=1)5d_{5/2}, J=\frac{3}{2}\rangle + 0.3[5p_{1/2}^{-1}5p_{3/2}^{-1}(J=1)5d_{3/2}, J=\frac{3}{2}\rangle$

deviate slightly more from the experiment than the positions of the $4d$ Auger lines. This is understandable, because the final-state interaction with the continuum, which is present in the first case but not in the second, has not been taken into account in the computations.

The most intensive lines in the measured energy spectrum are the lines 34, 38, 39, and 45 around 35 eV (Fig. 2). A comparison with the experimental spectrum of Xe (Ref. 9) and the calculated energy spectrum (Fig. 3) leads us to conclude that these lines are mainly due to the $4d^{-1}6s \rightarrow 4p^{-2}6s$ transitions. The splitting of the daughter lines in the presence of the outer $6s$ electron is insignificant both experimentally and theoretically. The intensity of the parent $4d^{-1} \rightarrow 4p^{-2}$, $^1S_0$ and $^1D_2$ lines [see, e.g., Xe (Ref. 9)] is thus mainly transferred to the lines 34 and 39 in the N_5 and to the lines 38 and 45 in the N_4 group. The parent lines $4d^{-1} \rightarrow 4p^{-2}$, $^3P_{0,1,2}$ lie on the high-energy side of these lines. The intensity ratio of the $4d_{5/2}$ and $4d_{3/2}$ transitions is of the order of 1.0. The determination of this ratio is not very accurate due to an overlap of the lines. The estimated ratio, however, deviates from the statistical distribution and from the result obtained for the $4d^{-1} \rightarrow 5p^{-1}x^{-1}$ transitions. The energy difference between experiment and theory is also slightly larger than in the case of the $4d^{-1} \rightarrow 5p^{-1}x^{-1}$ transitions. Some extra structure around the main lines also occurs. Owing to the near degeneracy of the configurations with $6s$ and $5d$ outer electrons, this extra structure may originate from the transitions with a pronounced $4d^{-1}5d \rightarrow 4p^{-2}5d$ character. These transitions gain their intensity through the configuration mixing effect.

The peak structure on the low-energy side of the main lines may originate from the inelastically scattered Auger electrons. According to the electron-energy-loss measurements,[16] the most intensive energy-loss doublet is separated by about 1.4 eV from the main peak.

A detailed interpretation of the $4d^{-1} \rightarrow 5p^{-1}x^{-1}$ and $4d^{-1} \rightarrow 5p^{-2}$ transitions is achieved in Tables III and IV. The energy-loss peaks associated with the main peaks are also indicated. The calculated energies refer to the Dirac-Fock ΔSCF results for the transitions $4d^{-1}(6s+5d) \rightarrow 5p^{-1}(6s+5d)^{-1}$ and $4d^{-1}(6s+5d) \rightarrow 5p^{-2}(6s+5d)$. Table IV also gives the final-state wave functions.

The high-energy electron beam used can also ionize the deeper M and N levels. Via the Auger decay, this can lead to the doubly ionized states where one of the holes is created in the $4d$ levels. The satellite Auger transitions, when these double-hole states decay to the triple-hole states, fall energetically on the low-energy side of the normal Auger transitions. Owing to the great number of overlapping multiplets, the satellite transitions are characterized by broad lines. Line 60 in the spectrum is probably due to the satellite transitions. The structure around 30 eV in the measured spectrum may also be interpreted as satellites. Broader linewidths were used in the fit of the experimental spectrum for these lines.

The peak structure around 20 eV originates from the $4d^{-1} \rightarrow 5s^{-1}5p^{-1}$ Auger transitions. The most intensive lines in this group should be due to the $4d_{3/2,5/2}^{-1} \rightarrow (5s^{-1}5p_{1/2,3/2}^{-1}, J=1)6s$, $J=\frac{1}{2}$, $\frac{3}{2}$ transitions (according to the $N_{4,5}O_1O_{2,3}\,^1P_1$ parent). If lines 12 and 15 in the experimental spectrum are interpreted as due to these transitions, an energy difference of 3.6 eV between experi-

ment and theory arises. The interaction with the final state of the satellite transitions may, however, considerably shift these lines. For example, the final state $5p^{-3}5d(6s+5d)$ of the satellites is nearly degenerated with the final state $5s^{-1}5p^{-1}(6s+5d)$ of the Auger decay. This is illustrated in Fig. 5 where the energy positions of the final-state configurations are depicted. Strong mixing of these configurations is hence possible. Detailed multiconfiguration calculations are needed before a less ambiguous interpretation of the fine structure at the energy region 20—30 eV is possible.

The peaks 54 and 55 on the high-energy side of the $4d^{-1}\rightarrow 5p^{-2}$ transitions are most probably due to autoionization. Strong autoionization peaks were observed in the $5p$ electron spectrum of barium following 2-keV electron impact.[2] The high-energy side of the $4d^{-1}\rightarrow 5s^{-1}5p^{-1}$ transitions may also contain autoionization lines, but their intensity may not be very high.

The binding energies of the $4d$ levels obtained from the Dirac-Fock ΔSCF calculations $E_B(N_4)=84.21$ eV and $E_B(N_5)=81.96$ eV agree reasonably well with the experimentally determined values $E_B(N_4)=85.07$ eV and $E_B(N_5)=82.79$ eV. The calculated $4d_{3/2}$-$4d_{5/2}$ spin-orbit splitting of 2.25 eV is in very good agreement with the experimental value of 2.26 eV determined as the mean value from the difference of the main lines in the N_5 and N_4 groups.

V. CONCLUSIONS

The configuration with the $4f$ outer electron, being less advantageous energetically in the initial and final states (see Fig. 5 for final state), does not seem to cause any remarkable effects on the observed fine structure. On the contrary, the $5d$ collapse clearly seems to be important in the studied spectrum. In the $4d^{-1}(6s+5d)$ initial state the lowest-lying levels were found to have a pronounced $6s$ character, whereas in the final state the levels with $6s$ and $5d$ outer electron match in energy. Experimental spectrum shows intensive lines corresponding to the transitions to the final-state levels with pronounced $6s$ character. Clear extra structure interpreted to the transitions to the levels with pronounced $5d$ character also appears in the Auger spectrum now studied.

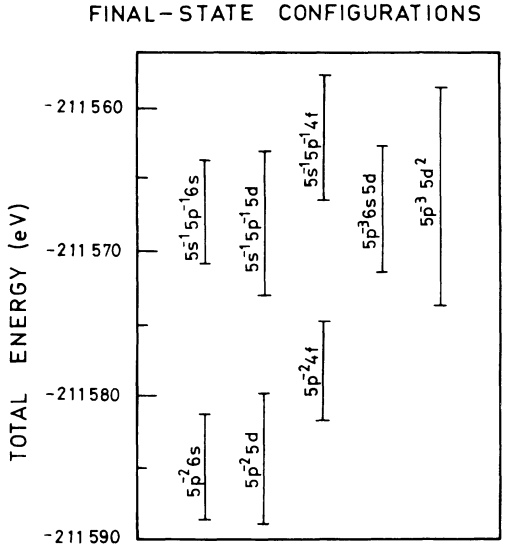

FIG. 5. Calculated energy positions of the final-state configurations of Auger and satellite transitions of Cs.

ACKNOWLEDGMENTS

This work has been supported by the Finnish Academy of Science. The authors wish to thank Hanna Pulkkinen and Matti Harkoma for assistance in the computations and in carrying out the experimental measurements.

[1]D. Rassi and K. J. Ross, J. Phys. B 13, 4683 (1980).
[2]W. Mehlhorn, B. Breuckmann, and D. Hausamann, Phys. Scr. 16, 177 (1977).
[3]R. A. Rosenberg, S. T. Lee, and D. A. Shirley, Phys. Rev. A 21, 132 (1980).
[4]J. P. Connerade, J. Phys. C 15, L367 (1982).
[5]J. P. Connerade, J. Phys. B 11, L409 (1978).
[6]J. P. Connerade and D. H. Tracy, J. Phys. B 10, L235 (1977).
[7]J. Väyrynen and S. Aksela, J. Electron Spectrosc. 16, 423 (1979).
[8]M. Tervonen, S. Aksela, and J. Väyrynen (unpublished).
[9]L. O. Werme, T. Bergmark, and K. Siegbahn, Phys. Scr. 6, 141 (1972).
[10]S. Ohtani, H. Nishimura, and H. Suzuki, Phys. Rev. Lett. 36, 863 (1976).
[11]J. E. Hansen and W. Persson, Phys. Rev. A 20, 364 (1979).
[12]J. Reader, Phys. Rev. A 13, 507 (1976).
[13]H. Petersen, K. Radler, B. Sonntag, and R. Haensel, J. Phys. B 8, 31 (1975).
[14]I. P. Grant, B. J. Kenzie, and P. H. Norrington, Comput. Phys. Commun. 21, 207 (1980); 21, 233 (1980).
[15]M. H. Chen, B. Crasemann, and H. Mark, Phys. Rev. A 24, 1158 (1981).
[16]I. V. Hertel and K. J. Ross, J. Phys. B 2, 484 (1968).